

Discrete and Continuous-time Soft-Thresholding with Dynamic Inputs

Aurèle Balavoine, *Student Member, IEEE*, Christopher J. Rozell, *Senior Member, IEEE*,
and Justin Romberg, *Senior Member, IEEE*,

Abstract

There exist many well-established techniques to recover sparse signals from compressed measurements with known performance guarantees in the static case. However, only a few methods have been proposed to tackle the recovery of time-varying signals, and even fewer benefit from a theoretical analysis. In this paper, we study the capacity of the Iterative Soft-Thresholding Algorithm (ISTA) and its continuous-time analogue the Locally Competitive Algorithm (LCA) to perform this tracking in real time. ISTA is a well-known digital solver for static sparse recovery, whose iteration is a first-order discretization of the LCA differential equation. Our analysis shows that the outputs of both algorithms can track a time-varying signal while compressed measurements are streaming, even when no convergence criterion is imposed at each time step. The ℓ_2 -distance between the target signal and the outputs of both discrete- and continuous-time solvers is shown to decay to a bound that is essentially optimal. Our analyses is supported by simulations on both synthetic and real data.

Index Terms

Iterative Soft-Thresholding, Locally Competitive Algorithm, Compressed Sensing, dynamical systems, ℓ_1 -minimization, tracking

I. INTRODUCTION

SPARSE recovery studies the problem of estimating a sparse signal from a set of linear measurements, when the measurements can potentially be highly undersampled. Mathematically, the problem consists in recovering a target signal $a^\dagger \in \mathbb{R}^N$ from noisy linear measurements $y = \Phi a^\dagger + \epsilon$ in \mathbb{R}^M , where ϵ is a noise vector and $\Phi \in \mathbb{R}^{M \times N}$ is the measurement matrix with $M \ll N$ in our scenario of interest. If the target is S -sparse, meaning that only S coefficients in a^\dagger are non-zero, a well-studied approach consists in solving an optimization program composed of a mean-squared error term and a sparsity-inducing term (typically measured using the ℓ_1 -norm $\|a\|_1 = \sum_i |a_i|$):

$$\arg \min_a \frac{1}{2} \|y - \Phi a\|_2^2 + \lambda \|a\|_1. \quad (1)$$

The Iterative Soft-Thresholding Algorithm (ISTA) is an algorithm that performs a discrete gradient step followed by a soft-thresholding operation at each iteration, while the Locally Competitive Algorithm (LCA) performs similar operations in a continuous-time dynamical system. Both algorithms have been shown to converge to the minimum of (1) when the target a^\dagger is static (see Sections II-B and II-A).

We extend this formulation to the problem where the target signal $a^\dagger(t)$ continuously evolves with time and generates time-varying measurements $y(t)$. While several approaches have been proposed to track a time-varying signal from compressed measurements (cf. Section II-C), they currently lack performance guarantees. Driven by the absence of theoretical analysis for the dynamic sparse recovery problem, we study the performance of the ISTA and the LCA when their inputs vary with time.

We set our analysis in the streaming setting (i.e., data is processed as it becomes available rather than in a batch computation), since recovering a time-varying sparse signal when the measurements are streaming at a high rate or computational resources are limited is of great interest for many applications. An example of such applications is networked control systems, where a controller receives measurements from and returns a control signal to a dynamically evolving system. For instance, in [1], the authors propose using an extension of ISTA to obtain a

The authors are with the School of Electrical and Computer Engineering, Georgia Institute of Technology, Atlanta, GA, 30332-0250 USA
Email: {aurele.balavoine,crozell,jrom}@gatech.edu.

This work was partially supported by NSF grants CCF-0905346 and CCF-0830456.

sparse control signal that can be sent efficiently through a rate-limited communication channel. As a consequence, in our analysis, the two algorithms may not reach a convergence criterion before the next measurement is received. While it has been previously observed in literature that limiting the number of iterations of certain algorithms in the streaming setting could still yield good convergence results (e.g., in [2]), no analysis has been previously provided for such iteration-limited settings.

The results of our analysis are given in Section III and show theoretically that both ISTA and LCA can track a time-varying target and reach a favorable error bound in the streaming setting, despite not being able to fully converge for each measurement. We show that the ℓ_2 -distance between the output and the target decays with a linear rate for ISTA, while it decays with an exponential rate for the LCA. These convergence rates match those obtained in the static setting. In addition, we show that the steady-state error for each algorithm is the static error plus a term that accounts for the dynamics in the problem (in particular, the energy in the derivative of the target and the time constant of the solver). Finally, in Section IV, we present the results of simulations on both synthetic and real data that support the mathematical findings.

II. BACKGROUND AND RELATED WORK

We start by giving a review of the ISTA discrete iteration and the continuous-time LCA network, along with a summary of the results obtained in the static case. We then look at what approaches have been taken for the dynamic recovery problem.

A. The Iterative Soft-Thresholding Algorithm

ISTA is one of the earliest digital algorithms developed for sparse recovery [3], and although it tends to converge slowly, many state-of-the-art solvers are only slight variations of its simple update rule [4]–[7]. Its update rule can be seen as a discretized generalized-gradient step for (1). At the l^{th} iterate, the output is denoted by $a[l] \in \mathbb{R}^N$ and the update rule is¹:

$$a[l+1] = T_\lambda (a[l] + \eta \Phi^T (y - \Phi a[l])). \quad (2)$$

The activation function $T_\lambda(\cdot)$ is the soft-thresholding function defined by:

$$a_n = T_\lambda(u_n) = \begin{cases} 0, & |u_n| \leq \lambda \\ u_n - \lambda z_n, & |u_n| > \lambda \end{cases}, \quad (3)$$

where $z_n = \text{sign}(u_n)$. The constant η represents the size of the gradient step, which is usually required to be in the interval $(0, 2 \|\Phi^T \Phi\|^{-1})$ to ensure convergence. Several papers have shown that ISTA converges to the solution a^* of (1) as l goes to infinity from any initial point $a[0]$ with linear rate [8], [9], i.e. $\exists d, \mathcal{K}$ such that $\forall l \geq 0$

$$\|a[l] - a^*\|_2 \leq \mathcal{K}d^l.$$

B. The Locally Competitive Algorithm

The LCA is a continuous-time system that was proposed in [10] to solve the ℓ_1 -minimization problem and other nonsmooth sparse recovery problems. Its simple and highly-parallel architecture makes it amenable to analog VLSI [11], [12]. The LCA is defined by a system of coupled, nonlinear Ordinary Differential Equations (ODEs) that controls the evolution over time of a network of nodes $u_n(t)$ for $n = 1, \dots, N$:

$$\begin{aligned} \tau \dot{u}(t) &= -u(t) - (\Phi^T \Phi - I) a(t) + \Phi^T y \\ a(t) &= T_\lambda(u(t)) \end{aligned}. \quad (4)$$

Each node or internal state variable is associated with a single dictionary element Φ_n , which corresponds to a column of the matrix Φ . The internal states produce output variables $a_n(t)$ for $n = 1, \dots, N$ through the activation function $T_\lambda(\cdot)$ applied entry-wise. The constant τ represents the time constant of the physical solver implementing

¹We indicate the iterate number l in brackets, to match the notation for the continuous time index, and the n^{th} entry of the vector in a subscript: $a_n[l]$.

the algorithm. A long lineage of research has shown that analog networks for optimization can have significant speed and power advantages over their digital counterparts [13]. Though ℓ_1 -minimization is our focus, previous work has shown that the LCA can be used to solve a wide class of optimization programs by varying the form of the activation function $T_\lambda(\cdot)$ [14]–[16]. For a wide class of activation functions, the LCA convergence is exponentially fast from any initial point $a(0)$ in the sense that $\exists d, \mathcal{K} > 0$, such that $\forall t \geq 0$

$$\|a(t) - a^*\|_2 \leq \mathcal{K}e^{-(1-d)t/\tau},$$

where $a^* = T_\lambda(u^*)$ is the solution of (1) [14]. Finally, the LCA output remains sparse when the target vector is sparse and the matrix Φ satisfies the restricted isometry property (RIP) [17]. In this scenario, the constant d can be approximated by the RIP constant of the matrix.

To make the link between the ISTA update rule and the LCA equation clear, we rewrite the ISTA iteration (2) as follows:

$$\begin{aligned} u[l+1] &= a[l] + \eta \Phi^T (y - \Phi a[l]) \\ a[l+1] &= T_\lambda(u[l+1]) \end{aligned}, \forall l \geq 0.$$

With this formulation, it is easy to see that ISTA is a first-order discretization of the LCA dynamics (or Euler method). Using a step size dl for the discretization equal to the LCA time-constant $dl = t_{l+1} - t_l = \tau$, the LCA ODE (4) becomes:

$$\begin{aligned} \tau \frac{u[l+1] - u[l]}{\tau} &= -u[l] + a[l] + \Phi^T (y - \Phi a[l]) \\ a[l+1] &= T_\lambda(u[l+1]), \end{aligned}$$

which can be written as

$$\begin{aligned} u[l+1] &= a[l] + \Phi^T (y - \Phi a[l]) \\ a[l+1] &= T_\lambda(u[l+1]). \end{aligned}$$

This matches the ISTA iteration for $\eta = 1$. Because ISTA is a discrete version of the LCA dynamics, we will perform simulations on a digital computer and simulate the LCA ODE using ISTA with the appropriate parameters. This allows us to compare existing approaches to ISTA and the LCA in Section IV by putting all the algorithms in the same framework.

C. Related work

Several approaches have been proposed to tackle the problem of tracking a high-dimensional sparse signal evolving with time from a set of undersample streaming measurements. Classical methods for tracking signals include Kalman filtering and particle filtering [18]. These methods require a reliable knowledge of the underlying dynamics of the target and do not exploit any sparsity information. Some recent papers have built on these methods by incorporating a sparsity-aware criteria, either via convex relaxation [19], [20] or greedy methods [2], and still require a priori knowledge of the target dynamics.

Another class of methods rely on building a probabilistic model for the evolution of the target's support and amplitudes, and use Bayesian inference techniques to estimate the next time sample [21]–[23]. These methods also necessitate a priori knowledge of the target's behavior to adjust several parameters. While [23] proposes estimating the model parameters online, it only does so in the non-causal smoothing case, which can become computationally expensive as the number of parameters is large.

Finally, the last class of methods is based on optimization. For instance, in [24], [25], an optimization program is set up to account for the temporal correlation in the target, and the recovery is performed in batches. In [26], the best dynamical model is chosen among a family of possible dynamics or parameters. In [27], a continuation approach is used to update the estimate of the target using the solution at the previous time-step. In [28]–[31], the optimization is solved using low-complexity iterative schemes. Unfortunately, all of the above methods lack strong theoretical convergence and accuracy guarantees in the dynamic case. Finally, in [32], a very general projection-based approach is studied. A convergence result is given but it is not clear how the necessary assumptions apply in the time-varying setting and it does not come with an accuracy result.

The ISTA and LCA belong to the class of optimization-based schemes. The two algorithms do not rely on any model of the underlying dynamics, and a minimal number of parameters need to be adjusted that are already present in the static case. In our analysis, convergence to the minimum of the objective in (1) or to a stopping criterion is not required. Rather, the LCA output evolves continuously with time as the input is streaming, while the standard ISTA iteration is performed as new measurements become available. This is particularly useful in scenarios where signals are streaming at very high rates or computational resources are limited. Despite this simple setting, our analysis shows that the LCA and ISTA can both track a moving target accurately and provides an analytic expression for the evolution of the ℓ_2 -distance between the output of both algorithms and the target.

III. TRACKING A TIME-VARYING INPUT

In this section, we present the target signal model and state the two main theorems that analyze the tracking abilities of the ISTA and LCA when recovering a time-varying input $a^\dagger(t)$.

A. Notations

We split the indices of the states and outputs into two sets. For $n \in \Gamma(t)$, called the *active set*, the states satisfy $|u_n(t)| > \lambda$ and the output $a_n(t)$ is strictly non-zero. For indices n in the *inactive set* $\Gamma^c(t)$, the states satisfy $|u_n(t)| \leq \lambda$ and the output $a_n(t)$ is zero. We call the corresponding nodes *active* and *inactive* respectively. Similarly, the support of the non-zero coefficients in $a^\dagger(t)$ is denoted as $\Gamma_\dagger(t)$. We also define the set $\Delta(t)$ that contains the q indices with largest amplitude in $|u(t)|$. While those three sets change with time as the target and algorithms evolve, for the sake of readability and when it is clear from the context, we omit the dependence on time in the notation.

We denote by $\Phi_{\mathcal{T}}$ the matrix composed of the columns of Φ indexed by the set \mathcal{T} , setting all the other entries to zero. Similarly, $u_{\mathcal{T}}$ and $a_{\mathcal{T}}$ refer to the elements in the original vectors indexed by \mathcal{T} setting other entries to zero.

Finally, we define the sequence $\{t_k\}_{\{k \in \mathbb{N}\}}$ of *switching times* for the LCA such that $\forall t \in [t_k, t_{k+1})$, the sets $\Gamma(t)$ and $\Gamma_\dagger(t)$ are constant. In other words, a switch occurs if either an entry leaves or enters the support of the output $a(t)$, in which case $\Gamma(t)$ changes, or if an entry leaves or enters the support of $a^\dagger(t)$, in which case $\Gamma_\dagger(t)$ changes.

In the following, the quantities C_k refer to distinct constants that do not depend on time, and that are indexed by k in order of appearance.

B. Signal model

In the continuous case, we assume that the underlying target signal $a^\dagger(t)$ and the noise vector $\epsilon(t)$ evolve continuously with time. As a consequence, the input $y(t)$ to the LCA is

$$y(t) = \Phi a^\dagger(t) + \epsilon(t), \quad \forall t \geq 0, t \in \mathbb{R}, \quad (5)$$

which is also continuous with time. The input to the discrete-time ISTA at iteration l is a sampled version of this continuous-time signal:

$$y[l] = \Phi a^\dagger[l] + \epsilon[l], \quad \forall l \geq 0, l \in \mathbb{Z}, \quad (6)$$

with sampling period T_s , so that $a^\dagger[l] = a^\dagger(l \cdot T_s)$. Letting dl denote the time to perform one ISTA iteration, we state all of our results in terms of the quantities dl and P , where $P \geq 1$ is the number of ISTA iterations performed between each new measurement, so that $T_s = P \cdot dl$. Since there is no additional information about the target between two measurements, the discrete target signal $a^\dagger[l]$ is modeled as a zero-hold version of the samples. We keep track of two indices: k indexes the latest measurement received and i indexes the number of ISTA iterations performed since the last measurement. Then any iteration l can be expressed as $l = kP + i$ with $0 \leq i \leq P - 1$. This is illustrated in Fig. 1. With our model, iterations between new measurements that are indexed by $kP \leq l \leq (k + 1)P - 1$ satisfy

$$a^\dagger[l] = a^\dagger[kP],$$

or equivalently

$$a^\dagger[kP + i] = a^\dagger[kP], \quad \forall k \geq 0, \forall i = 0, \dots, P - 1. \quad (7)$$

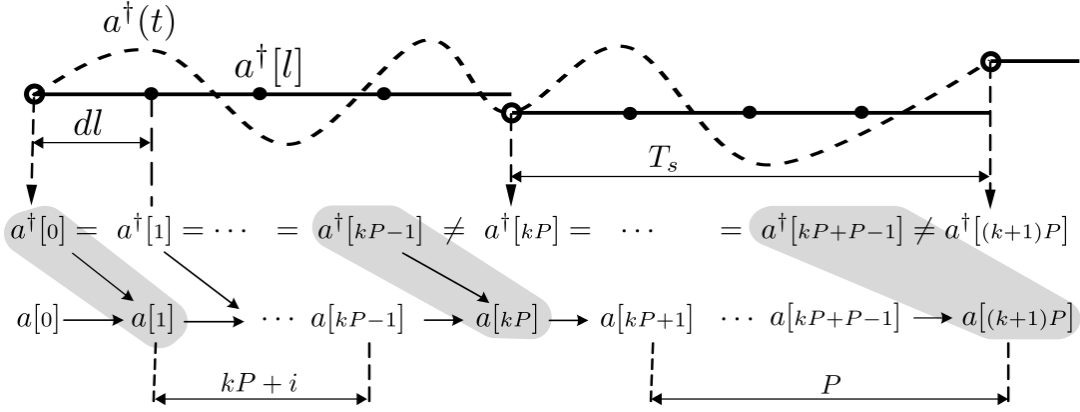


Fig. 1. Measurements of the continuous-time signal $a^\dagger(t)$ (dotted line) are continuously fed in input to the LCA. A measurement of the discrete version $a^\dagger[l]$ (filled dots on the straight line) is received every P^{th} ISTA iterates (corresponding to the empty circles). k indexes the number of measurements received and i indexes the number of ISTA iterations since the last measurement. The quantity of interest is $\|a[kP] - a^\dagger[kP - 1]\|_2$ (in grey), which represents the last error before a new measurement is received.

We focus on scenarios where the target signal is S -sparse (i.e., $|\Gamma_\dagger(t)| \leq S$, for all $t \geq 0$ and $|\Gamma_\dagger[l]| \leq S$, for all $l \geq 0$). We also require conditions on the energy in the target and its derivative. In the continuous case, our analysis requires that there exists $\mu \geq 0$ such that

$$\left\| \dot{a}^\dagger(t) \right\|_2 + \frac{1}{\tau} \left\| a^\dagger(t) \right\|_2 \leq \mu \quad \forall t \geq 0. \quad (8)$$

Intuitively, for a fixed μ , the more energy is present in the target or the smaller the time constant τ of the solver is, the slower the target needs to vary for the LCA to track it. A consequence of condition (8) is that the energy in the time-derivative is bounded by

$$\left\| \dot{a}^\dagger(t) \right\|_2 \leq \mu, \quad \forall t \geq 0,$$

and the energy of the target itself is bounded (see Lemma 3 in Appendix B):

$$\left\| a^\dagger(t) \right\|_2 \leq \beta, \quad \forall t \geq 0,$$

where $\beta = \max \left\{ \left\| a^\dagger(0) \right\|_2, \tau \mu \right\}$. In the discrete case, these conditions simply become

$$\left\| a^\dagger[l] \right\|_2 \leq \beta, \quad \forall l \geq 0, \quad (9)$$

and, for all $k \geq 0$,

$$\begin{aligned} \left\| a^\dagger[kP] - a^\dagger[kP - 1] \right\|_2 &= \left\| \int_{t_{kP-1}}^{t_{kP}} \dot{a}^\dagger(t) dt \right\|_2 \\ &\leq \int_{t_{kP-1}}^{t_{kP}} \left\| \dot{a}^\dagger(t) \right\|_2 dt \\ &\leq \int_{t_{kP-1}}^{t_{kP}} \mu dt = \mu dl, \end{aligned} \quad (10)$$

where again $dl = t_{l+1} - t_l$ is the time to perform one ISTA iteration. Note that because the measurement vector $y[l]$ changes every P^{th} iteration, ISTA never converges to the optimum of (1) if P is small. This approach is of great interest for scenarios where the measurements are streaming at very high rates.

Finally, we assume that the energy of the noise vector remains bounded and define σ as:

$$\|\epsilon(t)\|_2 \leq \left(\sqrt{1 + \delta} \right)^{-1} \sigma \quad \forall t \geq 0. \quad (11)$$

Our analysis remains valid in the noise-free case, when $\epsilon = 0$.

We assume throughout that the columns of Φ have unit norm: $\|\Phi_n\|_2 = 1$ and that Φ satisfies the Restricted Isometry Property (RIP) with parameter $(S + q, \delta)$, for some $q \geq 0$. This means that for all $(S + q)$ -sparse x in \mathbb{R}^N :

$$(1 - \delta) \|x\|_2^2 \leq \|\Phi x\|_2^2 \leq (1 + \delta) \|x\|_2^2. \quad (12)$$

In particular $\Phi = I$ satisfies (12) with $\delta = 0$, and so direct observations of the target satisfy our requirements.

C. Tracking abilities of ISTA

This section presents the tracking abilities of ISTA in the streaming setting. In the static setting, ISTA was shown in [8] to converge with a linear rate to the solution of the ℓ_1 -minimization program, for which an accuracy analysis was carried out in [33]. Combining these two results yields an ℓ_2 -error of the following form $\forall l \geq 0$:

$$\|a[l] - a^\dagger\|_2 \leq C_0 \tilde{c}^l + C_1,$$

where $\tilde{c} \in (0, 1)$ and $C_0, C_1 \geq 0$. The constant C_1 represents the steady-state error $\|a^* - a^\dagger\|$, where a^* is the solution of (1), and satisfies

$$C_1 \leq C_2 \lambda \sqrt{q} + C_3 \sigma,$$

where $q \geq 0$ (is typically on the order of S) and $C_2, C_3 \geq 0$. In the streaming setting, we show below that the decay of the ℓ_2 -distance between the target signal and the output of ISTA is still linear. For appropriate parameter choices, our results show that there exist $c \in (0, 1)$ and two constants $C_4, C_5 \geq 0$ such that, for all iterations $l \geq 0$,

$$\|a[l+1] - a^\dagger[l]\|_2 \leq C_4 c^l + C_5.$$

The constant C_5 represents the steady-state error, after enough iterations, and satisfies

$$C_5 \leq C_6 \lambda \sqrt{q} + C_7 \sigma + C_8 \mu dl,$$

where $C_6, C_7, C_8, \mu \geq 0$. Thus, the steady-state error in the dynamic setting is simply the static error plus a term that accounts for the dynamic components of the problem.

More precisely, in the streaming setting, the ISTA l^{th} iterate is

$$\begin{aligned} u[l+1] &= a[l] + \eta \Phi^T (y[l] - \Phi a[l]) \\ a[l+1] &= T_\lambda(u[l+1]) \end{aligned}, \quad \forall l \geq 0 \quad (13)$$

and we have the following theorem.

Theorem 1: Assume that the dictionary Φ satisfies the RIP with parameters $(S + 2q, \delta)$ for some $q \geq 0$, and that the gradient step size η in (13) satisfies

$$0 < \eta < \frac{2}{1 + \delta}. \quad (14)$$

Define $c = |\eta - 1| + \delta \cdot \eta < 1$. If the target signal satisfies conditions (9) and (10), the initial point $a[0]$ contains less than q active nodes and the following two conditions hold

$$\|u_{\Delta[0]}[0]\|_2 \leq \lambda \sqrt{q} \quad (15)$$

$$\eta(1 + \delta)\beta + \eta\sigma \leq (1 - c)\lambda\sqrt{q}, \quad (16)$$

then

- 1) the output $a[l]$ never contains more than q active nodes (i.e., $|\Gamma[l]| \leq q \quad \forall l \geq 0$); and
- 2) the ℓ_2 -distance between the output and the target signal satisfies $\forall l \geq 0$, letting $i = (l \bmod P)$ (i.e., $l = kP + i$, with $0 \leq i \leq P - 1$)

$$\|a[l+1] - a^\dagger[l]\|_2 \leq c^l \left(\|a[1] - a^\dagger[0]\|_2 - W \right) + \frac{c^{i+1}}{1 - c^P} \mu dl + V, \quad (17)$$

where

$$V = (1 - c)^{-1} (\eta\sigma + \lambda\sqrt{q}), \quad (18)$$

$$W = \frac{c}{1 - c^P} \mu dl + V. \quad (19)$$

This theorem is proven in Appendix C by induction on l and gives a bound on the ℓ_2 -error between the output of ISTA and the target for every iteration $l = kP + i$. The constants C_4 through C_8 can be explicitly written as

$$C_4 = \left\| a[1] - a^\dagger[0] \right\|_2 - W$$

$$C_5 \leq \underbrace{(1 - c)^{-1} \lambda \sqrt{q}}_{=C_6} + \underbrace{(1 - c)^{-1} \eta \sigma}_{=C_7} + \underbrace{\frac{c}{1 - c^P} \mu dl}_{=C_8}$$

In addition, the result shows that at every P^{th} iteration before a new measurement is received, the ℓ_2 -distance between the output and the target signal is

$$\left\| a[kP] - a^\dagger[kP - 1] \right\|_2 \leq c^{kP-1} \left(\left\| a[1] - a^\dagger[0] \right\|_2 - W \right) + \frac{c^P}{1 - c^P} \mu dl + V.$$

This quantity remains bounded and converges as k goes to infinity towards the steady-state value

$$V + \frac{c^P}{1 - c^P} \mu dl = (1 - c)^{-1} (\lambda \sqrt{q} + \eta \sigma) + \frac{c^P}{1 - c^P} \mu dl$$

with a linear rate of convergence. This final value is what is expected with the first term $(1 - c)^{-1} (\lambda \sqrt{q} + \eta \sigma)$ corresponding to the error involved with solving (1). Together with the bound (16), these terms resemble those in Corollary 5.1 in [33] obtained for the static case. The additional term $c^P (1 - c^P)^{-1} \mu dl$ decays with P and corresponds to the error we expect from having a time-varying input. The larger the variations in the target, the larger μ is, which corresponds to a more difficult signal to track and a larger error. Conversely, the slower the target varies, the larger P and as expected, the smaller the final error is. When P goes to infinity, this additional term disappears.

The two conditions (15) and (16) have a similar form to the conditions of Theorem 3 in [17]. If there is no initial guess, then $u[0] = 0$ and (15) holds. Assuming Φ is a subgaussian random matrix for which the RIP constant $\delta \sim \sqrt{S/M \log(N/S)}$, a similar analysis to Section IV.B of [17] implies that (16) holds for a number of measurements on the order of $S \log(N/S)$.

Condition (14) on the gradient step-size is better than the traditional condition that requires $0 \leq \eta \leq 2 \|\Phi^T \Phi\|^{-1}$, because the proof of Theorem 1 uses the RIP together with the fact that the output remains q -sparse.

D. Tracking abilities of the LCA

In the static setting, The LCA was shown in [14] and [17] to converge exponentially fast to the solution of (1). For the appropriate parameter choices, the ℓ_2 -error can be expressed for all time $t \geq 0$ as

$$\left\| a(t) - a^\dagger \right\|_2 \leq C_9 e^{-vt} + C_1,$$

where $v \in (0, 1)$ and $C_9 \geq 0$. The constant C_1 is again the steady-state error achieved when solving (1). The theorem below shows that, in the streaming setting, the ℓ_2 -distance between the LCA output and the target signal for appropriate parameter choices can be written $\forall t \geq 0$ as

$$\left\| a(t) - a^\dagger(t) \right\|_2 \leq C_{10} e^{-vt} + C_{11}.$$

The constant C_{11} represents the steady state error and satisfies

$$C_{11} \leq C_{12} \lambda \sqrt{q} + C_{13} \sigma + C_{14} \tau \mu,$$

where $C_{12}, C_{13}, C_{14}, \mu \geq 0$ with $\|\dot{a}^\dagger(t)\|_2 \leq \mu$ for all $t \geq 0$ and τ is the time constant of the LCA. As a consequence, the convergence in the dynamic setting is still exponential and the steady-state error is composed of the static error plus a term that accounts for the dynamic components in the problem.

Theorem 2: Assume that the dictionary Φ satisfies the RIP with parameter $(S + q, \delta)$, for some $q \geq 0$. We define the following quantity that depends on the threshold λ , the noise energy bound σ , the energy bound on the target signal μ , the parameter q and the RIP constant δ :

$$D = (1 - \delta)^{-1} (\tau\mu + \sigma + \lambda\sqrt{q}). \quad (20)$$

If the target signal satisfies (8), the initial active set $\Gamma(0)$ contains less than q active nodes, and the following two conditions hold

$$\|u_{\Delta(0)}(0)\|_2 \leq \lambda\sqrt{q} \quad (21)$$

$$\delta \cdot \max \left\{ \|a(0) - a^\dagger(0)\|_2, D \right\} + \beta + \sigma \leq \lambda\sqrt{q}, \quad (22)$$

then

- 1) the output $a(t)$ never contains more than q active nodes (i.e., $|\Gamma(t)| \leq q \quad \forall t \geq 0$); and
- 2) the ℓ_2 -distance between the LCA output and the target signal satisfies $\forall t \geq 0$

$$\|a(t) - a^\dagger(t)\|_2 \leq e^{-(1-\delta)t/\tau} \|a(0) - a^\dagger(0)\|_2 + \left(1 - e^{-(1-\delta)t/\tau}\right) D. \quad (23)$$

This theorem is proven by induction on the sequence of switching times in Appendix D and shows that the ℓ_2 -distance between the LCA output and the target signal converges exponentially fast towards its final value D in (18). This bound is again what is expected for the problem. The first term $(1 - \delta)^{-1} (\lambda\sqrt{q} + \sigma)$ corresponds to the expected error when solving (1) as shown in [33], while the additional term $(1 - \delta)^{-1} \tau\mu$ corresponds to the error associated with recovering a time-varying signal. Again, we see that the error increases with μ , the energy of the variations in the target. Conversely, the error decreases with a decreasing τ , corresponding to a faster solver.

The steady state value D for the LCA is equal to the steady-state value obtained for ISTA when its parameters are chosen appropriately. When ISTA is considered as the discretization of the LCA, then the discretization step dl for the Euler method is equal to τ , $\eta = 1$ in (13), $P = 1$ and so $c = \delta$ as discussed in Section II-B. Then the steady-state value for ISTA becomes:

$$V + \frac{c^P}{1 - c^P} \mu dl \leq (1 - \delta)^{-1} (\tau\mu + \sigma + \lambda\sqrt{q}).$$

The initial conditions (21) and (22) are similar to the initial conditions of Theorem 3 in [17]. In particular, (21) holds when there is no initial guess (i.e., $u(0) = 0$) and a similar analysis to that of Section IV.B in [17] shows that the number of measurements for (22) to hold is on the order of $S \log(N/S)$ for classic CS matrices for which $\delta \sim \sqrt{S/M \log(N/S)}$.

A careful look at the proof in Appendix D reveals that the following condition is necessary for our analysis:

$$\left\| \dot{a}^\dagger(t) \right\|_2 + \frac{1}{\tau} \left\| a_{\Gamma^c}^\dagger(t) \right\|_2 \leq \mu \quad \forall t \geq 0.$$

This is less restrictive than (8) since as the LCA evolves, the output gets closer to the target signal and the energy in $\|a_{\Gamma^c}^\dagger(t)\|_2 = \|a_{\Gamma^c}^\dagger(t) - a_{\Gamma^c}(t)\|_2$ decreases (the equality comes from the fact that $\Gamma^c(t)$ is the inactive set of $a(t)$ by definition). However, because the set $\Gamma^c(t)$ changes with time and the sequence of active sets is not known in advance, this condition is difficult to verify a priori in practice.

As a final remark, the convergence rate of both continuous and discrete algorithms depend on the RIP constant δ of the matrix Φ . However, the condition on the RIP parameters $(S + 2q, \delta)$ is stronger in Theorem (1) (vs. $(S + q, \delta)$ in Theorem (2)). This is because the ISTA is a discrete-time algorithm and the set of active elements $\Gamma[l + 1]$ may differ by as much as q elements from the previous active set $\Gamma[l]$, while the changes are continuous in the case of the LCA.

IV. SIMULATIONS

In this section, we provide simulations that illustrate the previous theoretical results².

A. Synthetic data

We generate a sequence of sparse vectors $\{a^\dagger[l]\}_l$ for $l = 1, \dots, 40$ of length $N = 512$ with sparsity $S = 40$ and with up to 20 entries that are allowed to leave or enter the support in the following manner. First, we generate the sequence of time-varying amplitudes for the nonzero entries. For $l = 1$, $S = 40$ amplitudes are drawn from a normal Gaussian distribution and normalized to have norm β . With these initial samples calculated, 39 consecutive time samples are generated as

$$\alpha[l+1] = \sqrt{\frac{\beta^2 - \mu^2}{\beta^2}} \alpha[l] + \frac{\mu}{\sqrt{S}} v[l],$$

where $v[l]$ is a vector in \mathbb{R}^S with amplitudes drawn from a standard Gaussian distribution. Each sample $\alpha[l]$ in the sequence has energy equal to β in expectation and innovation with energy proportional to μ . A set of 30 random indices is selected and 30 of the sequences in $\{\alpha[l]\}_{l=1, \dots, 40}$ are assigned to the corresponding indices in $\{a^\dagger[l]\}_{l=1, \dots, 40}$. Finally, each of the 10 remaining sequences in $\{\alpha[l]\}_{l=1, \dots, 40}$ is assigned to two random indices in $\{a^\dagger[l]\}_{l=1, \dots, 40}$, and a sinusoidal envelope is generated that controls when each index is active. The first index is set to the product of the envelope with the sequence $\alpha[l]$ when the envelope is positive and zero otherwise. Likewise, the second index is set to the product of the envelope and sequence when the envelope is negative and zero otherwise. This configuration results in a smooth change in support, while also enforcing that exactly $S = 40$ elements are nonzero in $a^\dagger[l]$ at all times.

When they are not varied, we choose $\eta = 1$, $\mu = 0.8$ and $P = 1$. The measurement matrix Φ is 256×512 with entries drawn from a random normal Gaussian distribution and columns normalized to 1. A Gaussian white noise with standard deviation $0.3 \|\Phi a^\dagger[0]\|_2 / \sqrt{M}$ is added to the measurements. This corresponds to a moderate level of noise. In Fig. 2, we plot the average over 1000 such trials of the ℓ_2 -error $\|a[kP] - a^\dagger[kP-1]\|_2$. We observe that the curves tend to a final value that matches the steady-state behavior $c^P (1 - c^P)^{-1} \mu dl$ predicted by theorem 1 as k goes to infinity. A higher value of P or a lower value of μ yields a lower steady-state. To verify that the theorem captures the correct behavior, we also plot on Fig. 3 the steady-state value as a function of P for $\mu = 0.8$ and find the parameters c and V so that the predicted function $c^P (1 - c^P)^{-1} \mu dl + V$ best fits the data. As the figure shows, this function seems to represent the steady-state behavior well.

Next, we vary the threshold λ and the sparsity level S , and for each pair generate 10 time samples of $a^\dagger[k]$ and associated measurements $y[k]$ in the same fashion as above. We run ISTA for $P = 5$ iterations per measurement. In Fig. 4, we plot the average over 100 such trials of the ratio of the maximum number of non-zero elements q in $a[l]$ over the sparsity level S . The plot shows that the maximum number of non-zero elements remains small (q is mostly contained between $1S$ and $10S$), which matches the theorems' prediction. The curve superimposed shows that λ and S obey a relationship of the form $\lambda = C/\sqrt{S}$, as expected from conditions (16) and (22).

B. Real Data

Finally, we test how ISTA performs in the streaming setting on real data and compare it against SpaRSA, a state-of-the-art LASSO solver [7], BPDN-DF that adds a time-dependent regularization between frames, RWL1-DF which additionally performs reweighting at each iteration [20] and DCS-AMP that uses a probabilistic model to describe the target's evolution [23]. We use 13 videos of natural scenes and randomly select 100 random sequences of 40 frames³. Since natural images are sparse in wavelet basis, following the work in [34], we use $\Phi = AB$ as the measurement matrix, where A consists of $M = 0.25N$ random rows of a noiselet matrix and B is a dual-tree discrete wavelet transform (DT-DWT) [35]. SpaRSA and BPDN-DF are given the previous solution as a warm start for the following frame. The results obtained for ISTA with $P = 1$ and $\eta = 1$ simulate the LCA ODE's.

²Matlab code running the experiments in this section can be downloaded at <http://users.ece.gatech.edu/~abalavoine3/code>

³The videos used can be downloaded at <http://trace.eas.asu.edu/yuv/>

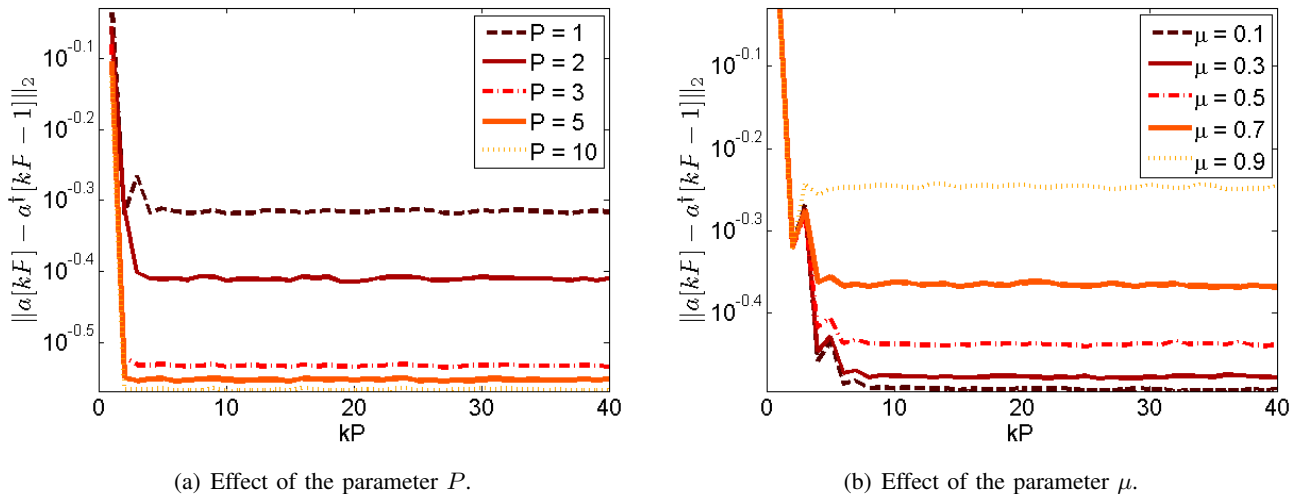


Fig. 2. ℓ_2 -distance between the target and the output at the P^{th} ISTA iterations.

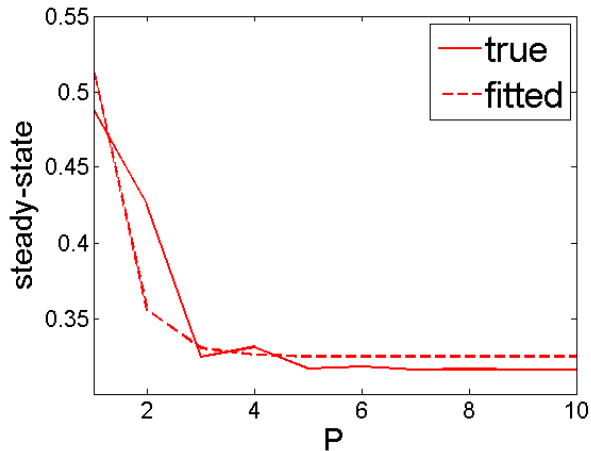


Fig. 3. Steady-state of the ISTA as it recovers synthetic time-varying signals and best fit of the function $c^P (1 - c^P)^{-1} \mu dl + V$ as a function of P .

In Fig. 5(a), we plot the relative mean-squared error, defined by $rMSE[k] = \frac{\|a[k] - a^\dagger[k]\|_2}{\|a^\dagger[k]\|_2}$, and the number of products by the matrix Φ or its transpose in Fig. 5(b), averaged over the 100 trials. We use the number of products by Φ and Φ^T rather than CPU time because it is a less arbitrary measure of the computational complexity for each algorithm. Figure 5(a) shows that the average rMSE values for ISTA with $P = 3$ and $P = 10$ reach a similar value to the rMSEs for SpaRSA and BPDN-DF after about 19 and 6 frames respectively. The average rMSE for ISTA with $P = 1$ converges much slower. The rMSE for RWL1-DF is much lower, due to the additional reweighting steps, however, the complexity for this method is much larger than the other four. While the complexity of ISTA for $P = 10$ is similar to the ones for SpaRSA, BPDN-DF and DCS-AMP, the complexity for $P = 3$ and $P = 1$ can be much smaller than any of the other approaches. In addition, ISTA only requires that two parameters be adjusted λ and η , while DCS-AMP has approximately 10.

V. CONCLUSIONS

The two main results of this paper provided an analysis for both the discrete-time ISTA and the continuous-time LCA in the context of the online recovery of a time-varying signal from streaming compressed measurements. Contrary to traditional approaches that require convergence or a stopping criterion before moving on to recover

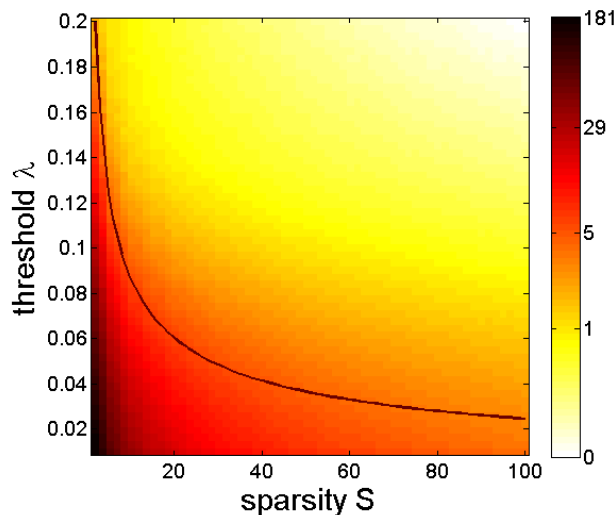


Fig. 4. Ratio of the maximum number of non-zero elements q over the sparsity level S for several values of λ and S averaged over 100 trials. The curve superimposed represents the best fit of the form $\lambda = C/\sqrt{S}$ of the curve for which $q = 4$ is constant.

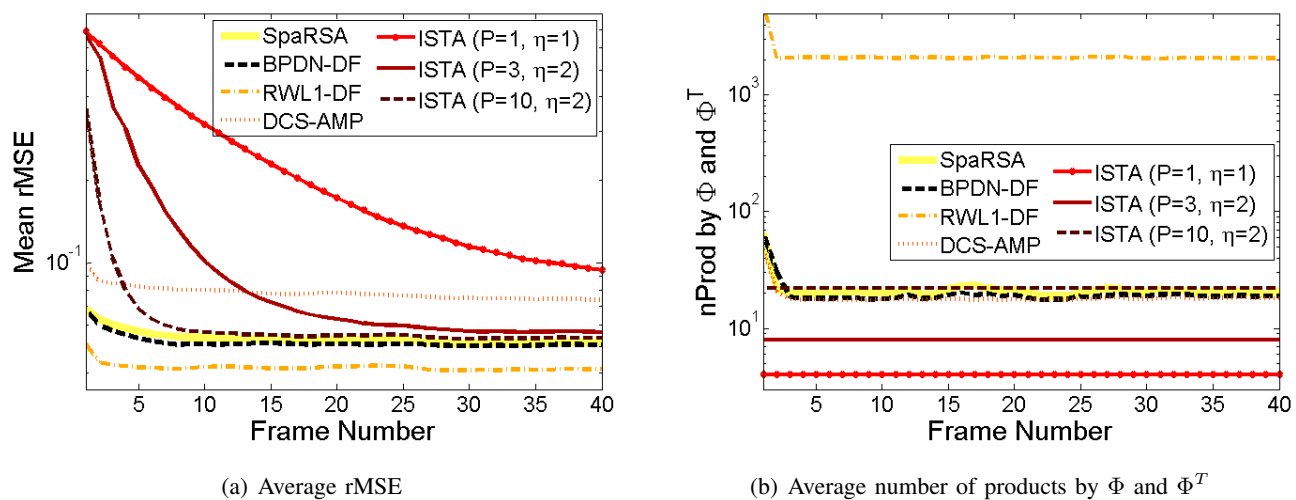


Fig. 5. Results of the experiment to recover the wavelet coefficients averaged over 100 random video sequences of 40 consecutive frames.

the next frame, we studied the outputs of the LCA and ISTA when their evolution rate is dictated by the rate at which measurements are streaming. Our results show that both algorithms are able to track a time-varying target in this setting. We believe that the techniques developed in this paper will prove useful for the analysis of other algorithms that currently lack theoretical analysis, in particular iterative-thresholding schemes that extend the classic ISTA. The results presented are particularly relevant for applications where the recovery needs to be performed in real-time and the signals are sampled at high rates or the computational resources are limited. While the simulations of the LCA ODE's with the appropriate parameters suggest that its convergence is slow, one would expect its time constant to be actually much faster in an actual analog system, so that the actual behavior would be closer to the one for ISTA with $P = 10$ (corresponding to an analog constant 10 times smaller than the digital equivalent). If this is the case, an analog implementation of the LCA has the potential to lead to a real-time and low-power solver for such challenging situations.

APPENDIX A
DIFFERENTIAL EQUATIONS

We will use the following results on differential equations freely in the proofs.

Lemma 1: If $x(\cdot) : \mathbb{R}^+ \rightarrow \mathbb{R}$ satisfies

$$\begin{aligned} \frac{dx(t)}{dt} &\leq -ax(t) + F(x(t), t), \\ x(0) &= x_0, \end{aligned}$$

then $\forall t \geq 0$:

$$x(t) \leq e^{-at}x_0 + e^{-at} \int_0^t e^{as} F(x(s), s) ds. \quad (24)$$

Proof: To show this, we compute $\forall t \geq 0$

$$\begin{aligned} \frac{d}{dt} (e^{at}x(t)) &= ae^{at}x(t) + e^{at} \frac{d}{dt} (x(t)) \\ &\leq ae^{at}x(t) + e^{at} (-ax(t) + F(x(t), t)) \\ &\leq e^{at} F(x(t), t). \end{aligned}$$

Integrating on both sides from 0 to t (using the positivity of the integral) yields

$$e^{at}x(t) - x(0) \leq \int_0^t e^{as} F(x(s), s) ds.$$

Thus:

$$x(t) \leq e^{-at}x_0 + e^{-at} \int_0^t e^{as} F(x(s), s) ds, \quad \blacksquare$$

APPENDIX B
LEMMAS

The following lemmas are also used in the proofs. The first one is a consequence of the RIP property in (12).

Lemma 2: If Φ satisfies the RIP with parameters $(S + q, \delta)$, the set Γ_1 contains less than q indices and the set Γ_2 contains less than S indices, then $\forall x \in \mathbb{R}^N$ supported on $\Gamma_1 \cup \Gamma_2$ and $\forall y \in \mathbb{R}^N$, the following holds:

$$\begin{aligned} (1 - \delta) \|x\|_2^2 &\leq \|\Phi x\|_2^2 \leq (1 + \delta) \|x\|_2^2, \\ \|\Phi_{\Gamma_1}^T \Phi_{(\Gamma_1^c \cap \Gamma_2)} x\|_2 &\leq \delta \|x\|_2, \\ \|(I_{\Gamma_1} - \Phi_{\Gamma_1}^T \Phi_{(\Gamma_1 \cup \Gamma_2)}) x\|_2 &\leq \delta \|x\|_2, \\ \|\Phi_{\Gamma_1}^T y\|_2 &\leq \sqrt{1 + \delta} \|y\|_2. \end{aligned}$$

Proof: The RIP implies that the singular values of $\Phi_{(\Gamma_1 \cup \Gamma_2)}$ are contained between $\sqrt{1 - \delta}$ and $\sqrt{1 + \delta}$, which entails the first inequality. The singular values of $\Phi_{\Gamma_1}^T$ are contained between 0 and $\sqrt{1 + \delta}$, which implies the last inequality. Finally, the eigenvalues of $\Phi_{(\Gamma_1 \cup \Gamma_2)}^T \Phi_{(\Gamma_1 \cup \Gamma_2)}$ are contained between $(1 - \delta)$ and $(1 + \delta)$. For the second and third inequalities, it suffices to observe that $\Phi_{\Gamma_1}^T \Phi_{(\Gamma_1^c \cap \Gamma_2)}$ and $(I_{\Gamma_1} - \Phi_{\Gamma_1}^T \Phi_{(\Gamma_1 \cup \Gamma_2)})$ are submatrices of $(I_{(\Gamma_1 \cup \Gamma_2)} - \Phi_{(\Gamma_1 \cup \Gamma_2)}^T \Phi_{(\Gamma_1 \cup \Gamma_2)})$. As a consequence, their operator norm is bounded by the operator norm of the bigger matrix, which is:

$$\left\| I_{(\Gamma_1 \cup \Gamma_2)} - \Phi_{(\Gamma_1 \cup \Gamma_2)}^T \Phi_{(\Gamma_1 \cup \Gamma_2)} \right\| \leq \max \{ (1 + \delta) - 1, 1 - (1 - \delta) \} = \delta. \quad \blacksquare$$

The following lemma gives a bound on the energy of the target when its time-derivative satisfies (8).

Lemma 3: If the target signal $a^\dagger(t)$ is continuous and satisfies (8) for all $t \geq 0$ then, $\forall t \geq 0$

$$\begin{aligned} \|a^\dagger(t)\|_2 &\leq e^{-t/\tau} \left(\|a^\dagger(0)\|_2 - \tau\mu \right) + \tau\mu \\ &\leq \underbrace{\max \left\{ \|a^\dagger(0)\|_2, \tau\mu \right\}}_{=\beta}. \end{aligned}$$

Proof: It suffices to notice that

$$\frac{d}{dt} (\|x(t)\|_2) = \frac{\frac{d}{dt} (\|x(t)\|_2^2)}{2\|x(t)\|_2} = \frac{x(t)^T \dot{x}(t)}{\|x(t)\|_2} \leq \|\dot{x}(t)\|_2,$$

where the last inequality comes from the Cauchy-Schwartz inequality. Thus, (8) implies

$$\frac{d}{dt} \left(\|a^\dagger(t)\|_2 \right) \leq -\frac{1}{\tau} \|a^\dagger(t)\|_2 + \mu.$$

Since $a^\dagger(t)$ is continuous, we can apply Lemma 1 to obtain the first inequality. The second inequality immediately follows from the monotonicity of the exponential. ■

The final lemma shows that a certain bound on the energy of the q entries with largest absolute value Δ in $u(t)$ imposes that at most q nodes are active.

Lemma 4: If Δ contains the indices of the q entries with largest absolute values in $u(t)$ and

$$\|u_\Delta(t)\|_2 \leq \lambda\sqrt{q},$$

then the active set Γ corresponding to the non-zero elements in $a(t) = T_\lambda(u(t))$ is subset of Δ and contains less than q indices, i.e. $\Gamma \subset \Delta$ and $|\Gamma| \leq q$.

Proof: Since Δ contains the q nodes with largest absolute values in $u(t)$, then $\forall j \in \Delta^c$, we have

$$|u_j(t)| \leq \|u_\Delta(t)\|_2 / \sqrt{q} \leq \lambda.$$

As a consequence, nodes in Δ^c are below threshold, which shows that only the nodes in Δ can be non-zero in $a(t)$. ■

APPENDIX C PROOF OF THEOREM 1

Proof: We start by checking that $c < 1$. By (14), we have

$$\begin{aligned} \eta(1 + \delta) < 2 \text{ and } \delta < 1 &\Rightarrow \eta\delta < \eta < 2 - \eta\delta \\ &\Rightarrow -1 + \eta\delta < \eta - 1 < 1 - \eta\delta \\ &\Rightarrow |\eta - 1| < 1 - \eta\delta \\ &\Rightarrow c < 1. \end{aligned}$$

In a first step, we show that

$$\|u[l]_{\Delta[l]}\|_2 \leq \lambda\sqrt{q}, \quad \forall l \geq 0 \tag{25}$$

by induction on l . If so, by Lemma 4, the active set contains less than q elements and 1) of the Theorem is proven. By (15), (25) holds for $l = 0$. Next, we assume that (25) holds for some $l \geq 0$. By Lemma 4, we have $\Gamma[l] \subset \Delta[l]$ and $|\Gamma[l]| \leq q$. As a consequence, the set

$$J = J[l+1] := \Delta[l+1] \cup \Gamma[l] \cup \Gamma_\dagger[l]$$

contains less than $S + 2q$ indices. Using the RIP of Φ , the eigenvalues of the matrix $\Phi_J^T \Phi_J$ are contained between $(1 - \delta)$ and $(1 + \delta)$ and

$$\begin{aligned} \|\eta\Phi_J^T \Phi_J - I_J\| &= \max \{ |\eta(1 + \delta) - 1|, |\eta(1 - \delta) - 1| \} \\ &= |\eta - 1| + \eta\delta = c. \end{aligned}$$

In addition, the form of the activation function (3) implies that $\|a[l]\|_2 \leq \|u_{\Gamma[l]}\|_2 \leq \|u_{\Delta[l]}\|_2 \leq \lambda\sqrt{q}$. Using (9) and hypothesis (16), we get

$$\begin{aligned} \|u_J[l+1]\|_2 &= \left\| \eta \Phi_J^T \Phi \left(a^\dagger[l] - a[l] \right) + a_J[l] + \eta \Phi_J^T \epsilon[l] \right\|_2 \\ &\leq \left\| \eta \Phi_J^T \Phi_J - I_J \right\|_2 \|a[l]\|_2 + \left\| \eta \Phi_J^T \Phi_J a^\dagger[l] \right\|_2 + \eta \left\| \Phi_J^T \epsilon[l] \right\|_2 \\ &\leq c \|a[l]\|_2 + \eta(1 + \delta) \left\| a^\dagger[l] \right\|_2 + \eta \sqrt{1 + \delta} \|\epsilon[l]\|_2 \\ &\leq c\lambda\sqrt{q} + \eta(1 + \delta)\beta + \eta\sigma \\ &\leq \lambda\sqrt{q}. \end{aligned}$$

Since $\Delta[l+1] \subset J[l+1]$, the induction hypothesis (25) holds at $l+1$. As a consequence, we proved 1) of the theorem and also the stronger result $\|u[l]_{J[l]}\|_2 \leq \lambda\sqrt{q}$, $\forall l \geq 1$, which will be used in the following.

Next, we show by induction on l that (17) holds $\forall l \geq 0$. It obviously holds for $l = 0$. Next, assume that for some $l \geq 0$, (17) holds. There exist a unique $k \geq 0$ and a unique $0 \leq i \leq P-1$ such that $l = kP + i$. In the previous part of the proof, we showed that $\|u_{J'}[l+2]\|_2 \leq \lambda\sqrt{q}$, where $J' = J[l+2] = \Delta[l+2] \cup \Gamma[l+1] \cup \Gamma_\dagger[l+1]$ and that J' contains less than $S + 2q$ indices. As a consequence, we can use the RIP of $\Phi_{J'}^T, \Phi_{J'}$ and get

$$\begin{aligned} \left\| a[l+2] - a^\dagger[l+1] \right\|_2 &\leq \left\| a[l+2] - u_{J'}[l+2] \right\|_2 + \left\| u_{J'}[l+2] - a^\dagger[l+1] \right\|_2 \\ &\leq \|u_{J'}[l+2]\|_2 + \left\| u_{J'}[l+2] - a^\dagger[l+1] \right\|_2 \\ &\leq \lambda\sqrt{q} + \left\| \eta \Phi_{J'}^T \epsilon[l+1] + (\eta \Phi_{J'}^T \Phi - I_{J'}) \left(a^\dagger[l+1] - a[l+1] \right) \right\|_2 \\ &\leq \lambda\sqrt{q} + \eta\sigma + c \left\| a^\dagger[l+1] - a[l+1] \right\|_2 \\ &\leq \lambda\sqrt{q} + \eta\sigma + c \left\| a[l+1] - a^\dagger[l] \right\|_2 + c \left\| a^\dagger[l] - a^\dagger[l+1] \right\|_2. \end{aligned}$$

We use the induction hypothesis (17) at l and split the analysis in two cases:

First case: When $i = P-1$, $l = (k+1)P-1$ and (10) yields $\left\| a^\dagger[l+1] - a^\dagger[l] \right\|_2 \leq \mu dl$. Thus,

$$\begin{aligned} \left\| a[l+2] - a^\dagger[l+1] \right\|_2 &\leq c \left(c^l \left[\left\| a[1] - a^\dagger[0] \right\|_2 - W \right] + \frac{c^P}{1-c^P} \mu dl + V \right) + c\mu dl + \lambda\sqrt{q} + \eta\sigma \\ &\leq c^{l+1} \left[\left\| a[1] - a^\dagger[0] \right\|_2 - W \right] + \frac{c^{P+1}}{1-c^P} \mu dl + cV + c\mu dl + \lambda\sqrt{q} + \eta\sigma \\ &\leq c^{l+1} \left[\left\| a[1] - a^\dagger[0] \right\|_2 - W \right] + \frac{c}{1-c^P} \mu dl + V. \end{aligned}$$

So the induction hypothesis (17) holds for $l+1 = (k+1)P$.

Second case: When $0 \leq i \leq P-2$, (7) yields $\left\| a^\dagger[l+1] - a^\dagger[l] \right\|_2 = 0$ and so

$$\begin{aligned} \left\| a[l+2] - a^\dagger[l+1] \right\|_2 &\leq c \left(c^l \left(\left\| a[1] - a^\dagger[0] \right\|_2 - W \right) + \frac{c^{i+1}}{1-c^P} \mu dl + V \right) + \lambda\sqrt{q} + \eta\sigma \\ &\leq c^{l+1} \left[\left\| a[1] - a^\dagger[0] \right\|_2 - W \right] + \frac{c^{i+2}}{1-c^P} \mu dl + cV + \lambda\sqrt{q} + \eta\sigma \\ &\leq c^{l+1} \left[\left\| a[1] - a^\dagger[0] \right\|_2 - W \right] + \frac{c^{i+2}}{1-c^P} \mu dl + V. \end{aligned}$$

Since $l+1 = kP + (i+1)$, with $1 \leq i+1 \leq P-1$, this proves the induction hypothesis (17) in the second case and finishes the proof. \blacksquare

APPENDIX D
PROOF OF THEOREM 2

Proof: We show by induction on the switching time t_k that the active set Γ_k contains less than q active elements and that equations (23) and

$$\|u_{\Delta(t)}(t)\|_2 \leq e^{-t/\tau} \|u_{\Delta(0)}(0)\|_2 + (1 - e^{-t/\tau}) \lambda\sqrt{q}, \quad (26)$$

hold $\forall t \leq t_k$.

At time $t_0 = 0$, the theorem hypotheses imply that Γ_0 contains less than q active elements, and that (23) and (26) hold.

Next, assume that $\forall t \leq t_k$ the active set contains less than q active elements and that (23) and (26) hold. We start by showing that (23) holds $\forall t \leq t_{k+1}$. By the induction hypothesis, the active set Γ contains less than q active nodes for all $t \leq t_k$, including the current active set Γ_k for $t \in [t_k, t_{k+1})$. As a consequence, the inequalities in Lemma 2 hold with $\Gamma_1 = \Gamma$ and $\Gamma_2 = \Gamma_{\dagger}$, for all $t \leq t_{k+1}$.

We compute the following time derivative $\forall t \leq t_{k+1}$:

$$\begin{aligned} \tau \frac{d}{dt} \left(\frac{1}{2} \|a(t) - a^\dagger(t)\|_2^2 \right) &= \tau (a(t) - a^\dagger(t))^T (\dot{a}(t) - \dot{a}^\dagger(t)) \\ &= (a(t) - a^\dagger(t))^T \left(-\Phi_\Gamma^T \Phi_\Gamma a(t) + \Phi_\Gamma^T y(t) - \lambda z_\Gamma - \tau \dot{a}^\dagger(t) \right) \\ &= - (a(t) - a^\dagger(t))^T \Phi_\Gamma^T \Phi_{(\Gamma \cup \Gamma_\dagger)} (a(t) - a^\dagger(t)) \\ &\quad + (a(t) - a^\dagger(t))^T \left(\Phi_\Gamma^T \epsilon(t) - \lambda z_\Gamma - \tau \dot{a}^\dagger(t) \right). \end{aligned}$$

Note that

$$\begin{aligned} &- (a(t) - a^\dagger(t))^T \Phi_\Gamma^T \Phi_{(\Gamma \cup \Gamma_\dagger)} (a(t) - a^\dagger(t)) \\ &= - \left\| \Phi_\Gamma (a(t) - a^\dagger(t)) \right\|_2^2 + (a(t) - a^\dagger(t))^T \Phi_\Gamma^T \Phi_{(\Gamma^c \cap \Gamma_\dagger)} a_{\Gamma^c}^\dagger(t) \\ &\leq - \left\| \Phi_\Gamma (a(t) - a^\dagger(t)) \right\|_2^2 + \|a_\Gamma(t) - a_\Gamma^\dagger(t)\|_2 \left\| \Phi_\Gamma^T \Phi_{(\Gamma^c \cap \Gamma_\dagger)} a_{\Gamma^c}^\dagger(t) \right\|_2 \\ &\leq -(1 - \delta) \|a_\Gamma(t) - a_\Gamma^\dagger(t)\|_2^2 + \delta \|a_\Gamma(t) - a_\Gamma^\dagger(t)\|_2 \|a_{\Gamma^c}^\dagger(t)\|_2 \\ &= -(1 - \delta) \|a(t) - a^\dagger(t)\|_2^2 + (1 - \delta) \|a_{\Gamma^c}^\dagger(t)\|_2^2 + \delta \|a_\Gamma(t) - a_\Gamma^\dagger(t)\|_2 \|a_{\Gamma^c}^\dagger(t)\|_2 \\ &\leq -(1 - \delta) \|a(t) - a^\dagger(t)\|_2^2 + \|a_{\Gamma^c}^\dagger(t)\|_2 \left((1 - \delta) \|a(t) - a^\dagger(t)\|_2 + \delta \|a(t) - a^\dagger(t)\|_2 \right) \\ &= -(1 - \delta) \|a(t) - a^\dagger(t)\|_2^2 + \|a_{\Gamma^c}^\dagger(t)\|_2 \|a(t) - a^\dagger(t)\|_2. \end{aligned}$$

Plugging this back in the expression for the time derivative, we obtain

$$\begin{aligned} &\tau \frac{d}{dt} \left(\frac{1}{2} \|a(t) - a^\dagger(t)\|_2^2 \right) + (1 - \delta) \|a(t) - a^\dagger(t)\|_2^2 \\ &\leq \|a(t) - a^\dagger(t)\|_2 \|a_{\Gamma^c}^\dagger(t)\|_2 + (a(t) - a^\dagger(t))^T \left(\Phi_\Gamma^T \epsilon(t) - \lambda z_\Gamma - \tau \dot{a}^\dagger(t) \right) \\ &\leq \|a(t) - a^\dagger(t)\|_2 \|a_{\Gamma^c}^\dagger(t)\|_2 + \|a(t) - a^\dagger(t)\|_2 \left\| \Phi_\Gamma^T \epsilon(t) - \lambda z_\Gamma - \tau \dot{a}^\dagger(t) \right\|_2 \\ &\leq \|a(t) - a^\dagger(t)\|_2 \|a_{\Gamma^c}^\dagger(t)\|_2 + \|a(t) - a^\dagger(t)\|_2 \left(\left\| \Phi_\Gamma^T \epsilon(t) \right\|_2 + \lambda \|z_\Gamma\|_2 + \tau \left\| \dot{a}^\dagger(t) \right\|_2 \right) \\ &\leq \|a(t) - a^\dagger(t)\|_2 \left(\|a_{\Gamma^c}^\dagger(t)\|_2 + \tau \left\| \dot{a}^\dagger(t) \right\|_2 \right) + \|a(t) - a^\dagger(t)\|_2 \left(\sqrt{1 + \delta} \|\epsilon(t)\|_2 + \lambda\sqrt{q} \right) \\ &\leq \|a(t) - a^\dagger(t)\|_2 (\tau\mu + \sigma + \lambda\sqrt{q}). \end{aligned}$$

Noting that

$$\frac{d}{dt} (\|x(t)\|_2) = \frac{\frac{d}{dt} (\|x(t)\|_2^2)}{2\|x(t)\|_2},$$

we obtain

$$\frac{d}{dt} \left(\|a(t) - a^\dagger(t)\|_2 \right) \leq -(1 - \delta)/\tau \|a(t) - a^\dagger(t)\|_2 + 1/\tau (\sigma + \lambda\sqrt{q} + \tau\mu).$$

Since $\|a(t) - a^\dagger(t)\|_2$ is continuous, we apply Lemma 1 and get $\forall t \leq t_{k+1}$:

$$\|a(t) - a^\dagger(t)\|_2 \leq e^{-(1-\delta)t/\tau} \|a(0) - a^\dagger(0)\|_2 + \left(1 - e^{-(1-\delta)t/\tau}\right) \frac{\sigma + \lambda\sqrt{q} + \tau\mu}{1 - \delta}.$$

This shows that (23) holds for all $t \leq t_{k+1}$.

We now show that (26) holds for all $t \leq t_{k+1}$. Note that, even though the set $\Delta(t)$ varies with time, $\|u_{\Delta(t)}(t)\|_2$ is continuous for all $t \geq 0$ (as a continuous function of supremum of continuous functions $|u_i(t)|$). Moreover, we can compute the time-derivative $\forall t \leq t_{k+1}$:

$$\begin{aligned} \tau \frac{d}{dt} \left(\frac{1}{2} \|u_{\Delta}(t)\|_2^2 \right) &= \tau u_{\Delta}(t)^T \dot{u}_{\Delta}(t) \\ &= u_{\Delta}(t)^T \left(-u_{\Delta}(t) + a_{\Delta}(t) - \Phi_{\Delta}^T \Phi a(t) + \Phi_{\Delta}^T y(t) \right) \\ &\leq -\|u_{\Delta}(t)\|_2^2 + \|u_{\Delta}(t)\|_2 \|\rho_{\Delta}(t)\|_2, \end{aligned}$$

where $\rho_{\Delta}(t) = a_{\Delta}(t) - \Phi_{\Delta}^T \Phi a(t) + \Phi_{\Delta}^T y(t)$. We can bound this quantity $\forall t \leq t_{k+1}$:

$$\begin{aligned} \|\rho_{\Delta}(t)\|_2 &= \|a_{\Delta}(t) - \Phi_{\Delta}^T \Phi a(t) + \Phi_{\Delta}^T y(t)\|_2 \\ &= \left\| a_{\Delta}^\dagger(t) + (I_{\Delta} - \Phi_{\Delta}^T \Phi) (a(t) - a^\dagger(t)) + \Phi_{\Delta}^T \epsilon(t) \right\|_2 \\ &\leq \|a^\dagger(t)\|_2 + \|\Phi_{\Delta}^T \epsilon(t)\|_2 + \|I_{\Delta} - \Phi_{\Delta}^T \Phi_{(\Delta \cup \Gamma_k)}\| \|a(t) - a^\dagger(t)\|_2 \\ &\leq \beta + \sigma + \delta \|a(t) - a^\dagger(t)\|_2, \end{aligned}$$

where we applied Lemma 2 with $\Gamma_1 = \Delta$ and $\Gamma_2 = \Gamma_{\dagger}$, and Lemma 3. Finally, applying bound (23) obtained for $\|a(t) - a^\dagger(t)\|_2$ for all $t \leq t_{k+1}$ and the monotonicity of the exponential, we get:

$$\begin{aligned} \|\rho_{\Delta}(t)\|_2 &\leq \beta + \sigma + \delta \left[e^{-(1-\delta)t/\tau} \|a(0) - a^\dagger(0)\|_2 + \left(1 - e^{-(1-\delta)t/\tau}\right) D \right] \\ &\leq \beta + \sigma + \delta \max \left\{ \|a(0) - a^\dagger(0)\|_2, D \right\} \\ &\leq \lambda\sqrt{q}, \end{aligned}$$

where the last inequality comes from the theorem's hypothesis (22). As a consequence, we obtained that $\forall t \leq t_{k+1}$:

$$\tau \frac{d}{dt} (\|u_{\Delta}(t)\|_2) \leq -\|u_{\Delta}(t)\|_2 + \lambda\sqrt{q}.$$

Using Lemma 1 again yields $\forall t \leq t_{k+1}$

$$\begin{aligned} \|u_{\Delta}(t)\|_2 &\leq e^{-t/\tau} \|u_{\Delta}(0)\|_2 + e^{-t/\tau} \int_0^t e^{\nu/\tau} \lambda\sqrt{q} d\nu \\ &\leq e^{-t/\tau} \|u_{\Delta}(0)\|_2 + \left(1 - e^{-t/\tau}\right) \lambda\sqrt{q}, \end{aligned}$$

which shows that (26) holds for all $t \leq t_{k+1}$.

Finally, we prove the last induction hypothesis, that the next active set Γ_{k+1} contains less than q indices. Since we proved that (26) holds $\forall t \leq t_{k+1}$, together with (21) this implies that:

$$\|u_{\Delta}(t_{k+1})\|_2 \leq e^{-t_{k+1}/\tau} \|u_{\Delta}(0)\|_2 + \left(1 - e^{-t_{k+1}/\tau}\right) \lambda\sqrt{q} \leq \lambda\sqrt{q}.$$

Applying Lemma 4 shows that the active set Γ_{k+1} contains less than q indices and finishes the proof. ■

REFERENCES

- [1] M. Nagahara, D.E. Quevedo, T. Matsuda, and K. Hayashi, "Compressive sampling for networked feedback control," in *IEEE Int. Conf. Acoust., Speech, Signal Process.*, Mar. 2012, pp. 2733–2736.
- [2] W. Dai, D. Sejdinovic, and O. Milenkovic, "Gaussian dynamic compressive sensing," in *Int. Conf. Sampling Theory and Appl.*, Singapore, 2011.
- [3] I. Daubechies, M. Defrise, and C. De Mol, "An iterative thresholding algorithm for linear inverse problems with a sparsity constraint," *Comm. Pure Appl. Math.*, vol. 57, no. 11, pp. 1413–1457, Aug. 2004.
- [4] A. Beck and M. Teboulle, "A fast iterative shrinkage-thresholding algorithm with application to wavelet-based image deblurring," in *IEEE Int. Conf. Acoust., Speech, Signal Process.*, 2009, pp. 693–696.
- [5] J. M Bioucas-Dias and M. A.T. Figueiredo, "A new TwIST: two-step iterative Shrinkage/Thresholding algorithms for image restoration," *IEEE Trans. Image Process.*, vol. 16, no. 12, pp. 2992–3004, Dec. 2007.
- [6] M. A. T. Figueiredo, R. D. Nowak, and S. J. Wright, "Gradient projection for sparse reconstruction: Application to compressed sensing and other inverse problems," *IEEE J. Sel. Topics Signal Process.*, vol. 1, no. 4, pp. 586–597, Dec. 2007.
- [7] S. J. Wright, R. D. Nowak, and M. A. T. Figueiredo, "Sparse reconstruction by separable approximation," *IEEE Trans. Signal Process.*, vol. 57, no. 7, pp. 2479–2493, 2009.
- [8] K. Bredies and D. A. Lorenz, "Linear convergence of iterative soft-thresholding," *J. Fourier Anal. Appl.*, vol. 14, no. 5-6, pp. 813–837, Dec. 2008.
- [9] E. T. Hale, W. Yin, and Y. Zhang, "Fixed-point continuation for ℓ_1 -minimization: Methodology and convergence," *SIAM J. Optim.*, vol. 19, no. 3, pp. 1107–1130, Jan. 2008.
- [10] C. J. Rozell, D. H. Johnson, R. G. Baraniuk, and B. A. Olshausen, "Sparse coding via thresholding and local competition in neural circuits," *Neural Comput.*, vol. 20, no. 10, pp. 2526–2563, Oct. 2008.
- [11] S. Shapero, A. S. Charles, C. J. Rozell, and P. Hasler, "Low power sparse approximation on reconfigurable analog hardware," *IEEE J. Emerg. Sel. Topic Circuits Syst.*, vol. 2, no. 3, pp. 530–541, Sept. 2012.
- [12] S. Shapero, C. J. Rozell, and P. Hasler, "Configurable hardware integrate and fire neurons for sparse approximation," *Neural Netw.*, 2013.
- [13] A. Cichocki and R. Unbehauen, *Neural Networks for Optimization and Signal Processing*, Wiley, 1993.
- [14] A. Balavoine, J. Romberg, and C. J. Rozell, "Convergence and rate analysis of neural networks for sparse approximation," *IEEE Trans. Neural Netw.*, vol. 23, no. 9, pp. 1377–1389, Sept. 2012.
- [15] A. Balavoine, C. J. Rozell, and J. Romberg, "Convergence of a neural network for sparse approximation using the nonsmooth Łojasiewicz inequality," in *Int. Joint Conf. Neural Netw.*, Dallas, TX, Aug. 2013.
- [16] A. S. Charles, P. Garrigues, and C. J. Rozell, "A common network architecture efficiently implements a variety of sparsity-based inference problems," *Neural computation*, vol. 24, no. 12, pp. 3317–3339, Dec. 2012.
- [17] A. Balavoine, C.J. Rozell, and J. Romberg, "Convergence speed of a dynamical system for sparse recovery," *IEEE Trans. Signal Process.*, vol. 61, no. 17, pp. 4259–4269, Jan. 2013.
- [18] Z. Chen, "Bayesian filtering: From kalman filters to particle filters, and beyond," 2003.
- [19] N. Vaswani, "Kalman filtered compressed sensing," in *IEEE Int. Conf. Image Process.*, Oct. 2008, pp. 893–896.
- [20] A. S. Charles and C. J. Rozell, "Dynamic filtering of sparse signals using reweighted ℓ_1 ," in *IEEE Int. Conf. Acoust., Speech, Signal Process.*, 2013, pp. 6451–6455.
- [21] D. Sejdinovic, C. Andrieu, and R. Piechocki, "Bayesian sequential compressed sensing in sparse dynamical systems," in *48th Annu. Allerton Conf. Commun., Control, Comput.*, 2010, pp. 1730–1736.
- [22] B. Shahrashi, A. Talari, and N. Rahnavard, "TC-CSBP: compressive sensing for time-correlated data based on belief propagation," in *45th Annu. Conf. Inf Sci. Syst.*, 2011, pp. 1–6.
- [23] J. Ziniel, L.C. Potter, and P. Schniter, "Tracking and smoothing of time-varying sparse signals via approximate belief propagation," in *2010 Conference Record of the Forty Fourth Asilomar Conference on Signals, Systems and Computers (ASILOMAR)*, 2010, pp. 808–812.
- [24] D. Angelosante, G.B. Giannakis, and E. Grossi, "Compressed sensing of time-varying signals," in *16th Int. Conf. Digit. Signal Process.*, 2009, pp. 1–8.
- [25] D. Angelosante, J.A. Bazerque, and G.B. Giannakis, "Online adaptive estimation of sparse signals: Where RLS meets the ℓ_1 -norm," *IEEE Trans. Signal Process.*, vol. 58, no. 7, pp. 3436–3447, 2010.
- [26] E. C. Hall and R. M. Willett, "Dynamical models and tracking regret in online convex programming," in *Int. Conf. Mach. Learn.*, Atlanta, 2013, vol. 28.
- [27] M. S. Asif and J. Romberg, "Dynamic updating for ℓ_1 minimization," *IEEE J. Sel. Topics Signal Process.*, vol. 4, no. 2, pp. 421–434, Apr. 2010.
- [28] Y.V. Zakharov and V.H. Nascimento, "DCD-RLS adaptive filters with penalties for sparse identification," *IEEE Trans. Signal Process.*, vol. 61, no. 12, pp. 3198–3213, June 2013.
- [29] K. Slavakis, Y. Kopsinis, and S. Theodoridis, "Adaptive algorithm for sparse system identification using projections onto weighted ℓ_1 balls," in *IEEE Int. Conf. Acoust., Speech, Signal Process.*, Mar. 2010, pp. 3742–3745.
- [30] B. Babadi, N. Kalouptsidis, and V. Tarokh, "SPARLS: the sparse RLS algorithm," *IEEE Trans. Signal Process.*, vol. 58, no. 8, pp. 4013–4025, Aug. 2010.
- [31] Y. Chen, Y. Gu, and A.O. Hero, "Sparse LMS for system identification," in *IEEE Int. Conf. Acoust., Speech, Signal Process.*, Apr. 2009, pp. 3125–3128.
- [32] K. Slavakis, Y. Kopsinis, S. Theodoridis, and S. McLaughlin, "Generalized thresholding and online sparsity-aware learning in a union of subspaces," *IEEE Trans. Signal Process.*, vol. 61, no. 15, pp. 3760–3773, Aug. 2013.

- [33] Tong Zhang, “Some sharp performance bounds for least squares regression with l1 regularization,” *Ann. Statist.*, vol. 37, no. 5A, pp. 2109–2144, 2009.
- [34] J. Romberg, “Imaging via compressive sampling,” *IEEE Sig. Process. Mag.*, vol. 25, no. 2, pp. 14–20, 2008.
- [35] I. W. Selesnick, R. G. Baraniuk, and N. C. Kingsbury, “The dual-tree complex wavelet transform,” *IEEE Signal Process. Mag.*, vol. 22, no. 6, pp. 123–151, 2005.